Magnetic fabrics under high-energy fluvial regime of the Himalayan Foreland Basin, NW Himalaya

G. Rathi[1], S. J. Sangode[1,2,*], Rohtash Kumar[1] and Sumit K. Ghosh[2]

[1]Wadia Institute of Himalayan Geology, Dehradun 248 001, India
[2]Present address: Department of Geology, University of Pune, Ganeshkhind, Pune 411 007, India

We present here magnetic fabric studies in a high-energy palaeochannel sequence of Nagri Formation (Late Miocene) of the Siwalik Group in the Himalayan Foreland Basin. Detailed studies on 47 well-exposed sites of primary sedimentary structures from a 1800 m thick sedimentary succession in Dehradun Sub-basin are made using anisotropy of magnetic susceptibility (AMS), rock magnetism, petrography and thermo-magnetic (fabric enhancement) analysis. The principle susceptibility ellipsoid axis (K_1) is sub-parallel to the palaeoflow direction due to anisotropy resultant of (i) poorly oriented ferrimagnetic grains, and (ii) fairly well-oriented paramagnetic mineral matrix. Thermal enhancement of fabrics primarily indicates oxidation of pre-existing antiferromagnetic and paramagnetic minerals along bedding planes into majority of ferrimagnetic oxides, resulting in the enhancement of degree of foliation.

This study indicates an extra-sensitive nature of the AMS to the paramagnetic matrix, giving rise to a resultant anisotropy that depends on the ratio of ferrimagnetic to paramagnetic minerals, their grain size, grain geometry, energy conditions and stream power. These factors in turn are governed by the hydrodynamic response to tectonic and climatic changes in the hinterland and basin. Thus we suggest a greater utility of magnetic fabrics as a high-resolution approach to quantify fluvial responses to tectonic and climatic changes.

Keywords: Anisotropy, Himalayan Foreland Basin, magnetic susceptibility, Nagri Formation, Siwalik Group.

PRIMARY fabrics preserved in sedimentary rocks are useful to estimate palaeohydrodynamic conditions by relating them to depositional environments and palaeoflow variabilities[1,2]. Quantitative estimates from sedimentary records thus have a great demand as input to study the hydrodynamic behaviour of dynamic river systems such as the Ganga, Brahmputra, Satluj and Yamuna in the frontal Himalayan fold thrust belt. Such information is essential to understand and reconstruct high-energy fluvial events such as palaeofloods, their genesis, frequency and evolutionary trends[1–6]. About 6 km thick sedimentary sequence in the Himalayan Foreland Basin (HFB) exposes several records of fluvial sequence in the time-span of the last ~15 Ma. These records are studied using classical approaches of field sedimentology[7–13] that are constrained in providing accurate palaeohydrodynamic information due to complex structural settings and rare 3D exposures of suitable primary sedimentary structures.

Anisotropy of magnetic susceptibility (AMS) is a high-resolution instrumental technique to reveal a 3D fabric based on standard analytical methods[14–17]. A symmetrical second-order tensor geometrically expressed by an ellipsoid is determined from the AMS fabric[14,16]. It represents statistical alignment of magnetic minerals, with the most magnetically susceptible minerals giving rise to shape orientation or lattice orientations governed by the kinematics or depositional history[14,15,17,18]. Hence variation in magnitude and direction of the magnetic fabrics either represents the strain experienced by the rock or the alignment of ferrimagnetic (magnetite, maghemite, titanomagnetite) and paramagnetic mineral grains (majority of pyroxene, amphiboles, feldspars and clay minerals) by ambient flow regimes[14,15,17,18]. Thus apart from its wider use as the strain indicator in deformed rocks, AMS can be used to infer flow-related parameters in sediments, volcanic rocks or emplacement-related fabrics in granites[14,15,17,18–23].

The primary fabrics in sedimentary rocks are influenced by various factors like grain geometries, depositional gradient, stream power and depositional environment[1,2,24]. This restricts a straightforward and universal application of AMS and demands case studies to be examined, especially in a dynamic set-up like the Himalaya. Previously, Sangode *et al.*[20,23] and Kumar *et al.*[10] attempted AMS studies in the Late Cenozoic Siwalik fluvial system of the HFB, that highlights the complexity and site-specific nature of the magnetic fabrics. These workers have suggested fabric variation from proximal to distal alluvial fan setting and its dependency over energy conditions that are in turn governed by tectonic impulses (thrust activation and reactivation) in the given hinterland set-up. However, these attempts were based upon a more generalized regional approach and there is a need for detailed site-

*For correspondence. (e-mail: sangode@rediffmail.com)

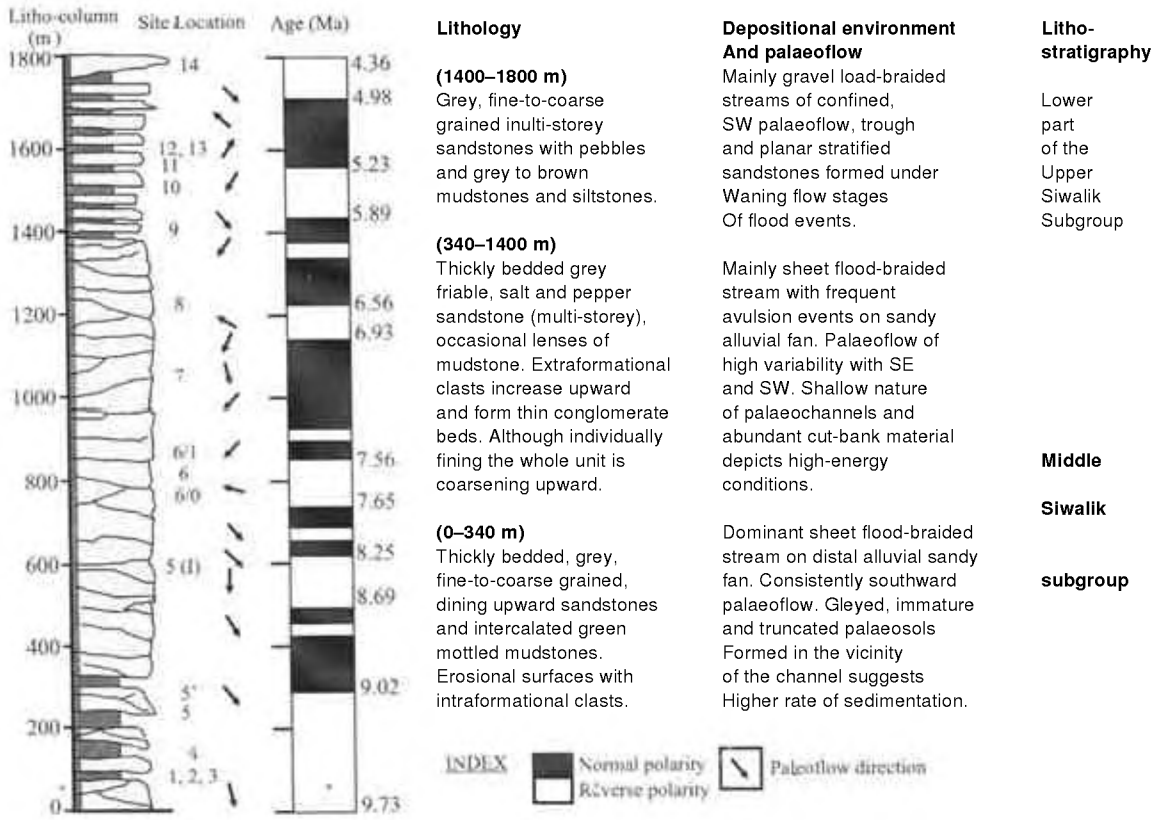

Figure 1. Composite litholog of the Mohand Rao section (details in Kumar *et al.*[9]) showing magnetostratigraphic column (age after Sangode *et al.*[23]) and brief description on lithology, depositional environment and stratigraphy. Arrows mark the palaeoflow direction based upon PSS.

specific approach to understand the fabric control of magnetic minerals. We present here such an attempt by specifically sampling the well-exposed primary sedimentary structures (PSS) that are indicative of palaeoflow directions in the widespread channel sedimentation of the Nagri Formation[7,8,10,11].

The Nagri Formation represents the most characteristic channel sedimentation in the Siwalik Group due to its widespread occurrence in the form of thickly bedded stacks of grey-coloured sandstones[7,8,10,11]. A detailed account of sedimentology and magnetostratigraphy for the Nagri channel sequence in the Mohand Rao (MR) and surrounding region of the Dehradun Sub-basin is available from previous work[9–13,23,25–27]. At MR, the channels are mainly represented by dominant sheet flood-braided streams over mid-to-distal sandy alluvial fan (Figure 1)[9–11].

We collected 47 oriented blocks from well exposed trough cross stratifications (37 TCS), ripple drift laminations (2 RD), planar cross stratifications (2 PCS) and horizontal laminations (5 HL) (Figure 2 *a–f*) from 1800 m thick sedimentary sequence along the MR near Dehradun (Figures 1–3). This article presents magnetic and petrographic studies and a comparison with the PSS-based upon 310 specimens prepared out of the 47 oriented block samples from 13 distinct sites of the PSS in the MR section.

Methods

Sampling was undertaken following the oriented block method[14]. Each block was cored and cut into specimens of 2.5 cm diameter and 2.2 cm height by retaining their field orientations. The specimens were finally washed with dilute HCl to remove machine contamination. A high-sensitivity Spinner version of the AGICO (Czech) KLY-3S Kappabridge anisotropy meter was used to measure the AMS for all the 310 specimens. Magnetic susceptibility in low (0.47 kHz) and high (4.7 kHz) frequency was measured (using Bartington's laboratory sensor) for a rough estimate on concentration and grain size of the ferrimagnetic mineral content. Isothermal remanent magnetization (IRM) was measured by inducing forward fields (up to 2000 mT) and back fields (up to –500 mT) at intervals of 10 to 100 mT. The analysis was performed using ASC impulse magnetizer and the Minispin rock magnetometer. An anhysteretic remanent magnetization (ARM) comparable to the earth's magnetic field was grown over a 100 mT peak

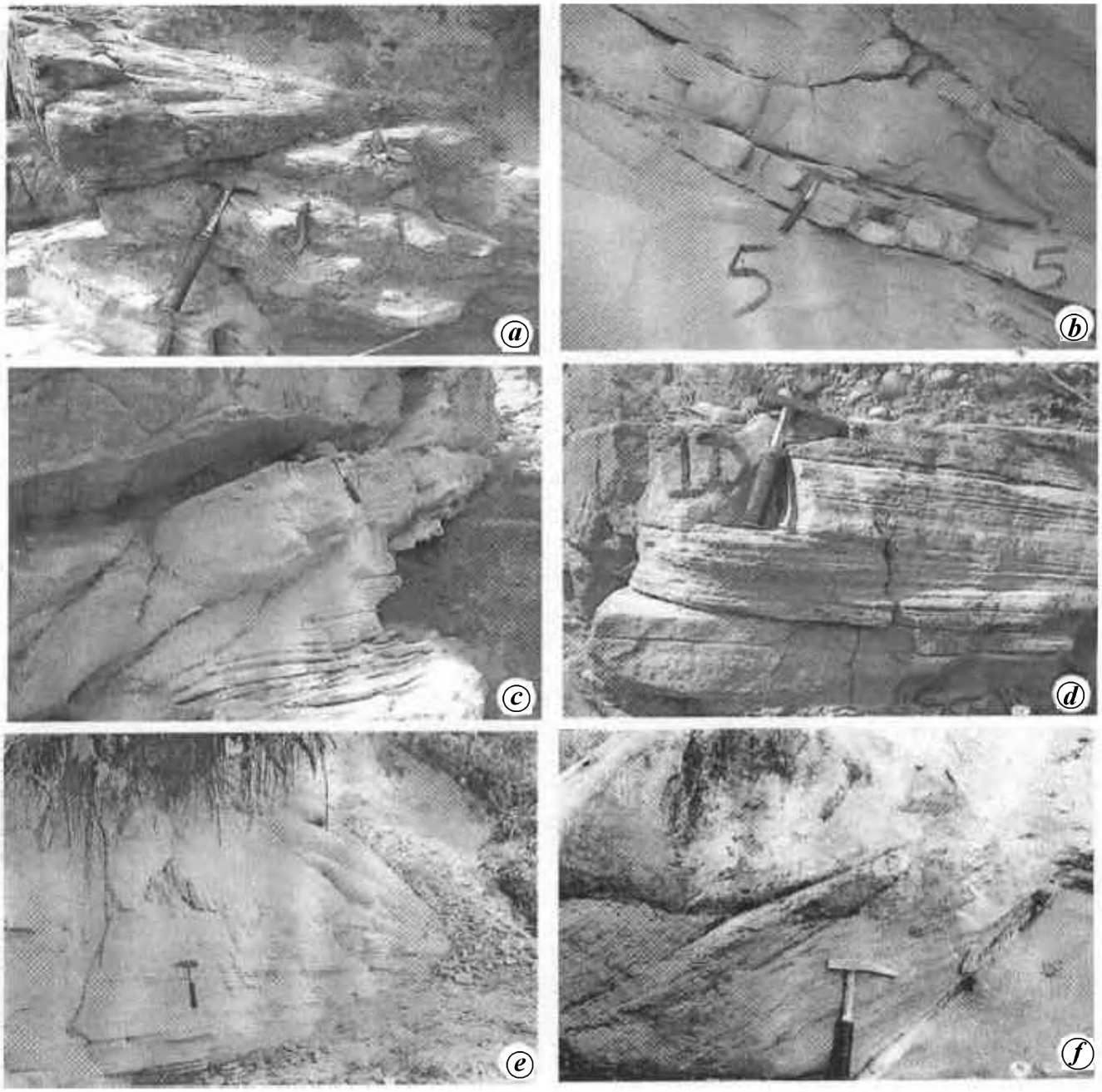

Figure 2. Photographs of some primary sedimentary structures in the litholog. ***a***, Trough cross-stratification (TCS) at site 1a between 0 and 200 m. ***b***, TCS at site 5 at 600 m height. ***c***, TCS (upper part) and planar cross-stratification (PCS; lower part, seen as bands) at site 2 between 0 and 200 m. ***d***, PCS at site 1D between 0 and 200 m height. ***e***, at PCS, some distance from site 2 between 0 and 200 m height. ***f***, Ripple drift lamination at site 11 between 1400 and 16000 m height.

demagnetizing field to know the proportion of stable ferrimagnetic grains using Molspin alternating field demagnetizer with ARM facility. These rock magnetic results (susceptibility, IRM and ARM) allowed to distinguish samples with varied magnetic mineral concentration and grain size (discussed later).

A batch of 22 representative samples was further selected for the thermal fabric enhancement study, for which a detailed rock magnetic analysis was made at room temperature and after heating to 700°C. The directions (declination and inclination) and magnitudes of the three principle susceptibility axes (K_1, K_2, K_3, where $K_1 \geq K_2 \geq K_3$) are derived using the computer program SUSAR, available with KLY-3S Kappabridge. This program further determines the degree of magnetic anisotropy (P_j) and shape parameter (T) using the equations given in Tarling and Hrouda[14]. P_j is the measure of eccentricity of susceptibility ellipsoid and T provides information on its shape. The latter varies between –1 and +1; for the oblate ellipsoid $T > 0$ for prolate ellipsoid T is less than 0 to –1. Since the rock

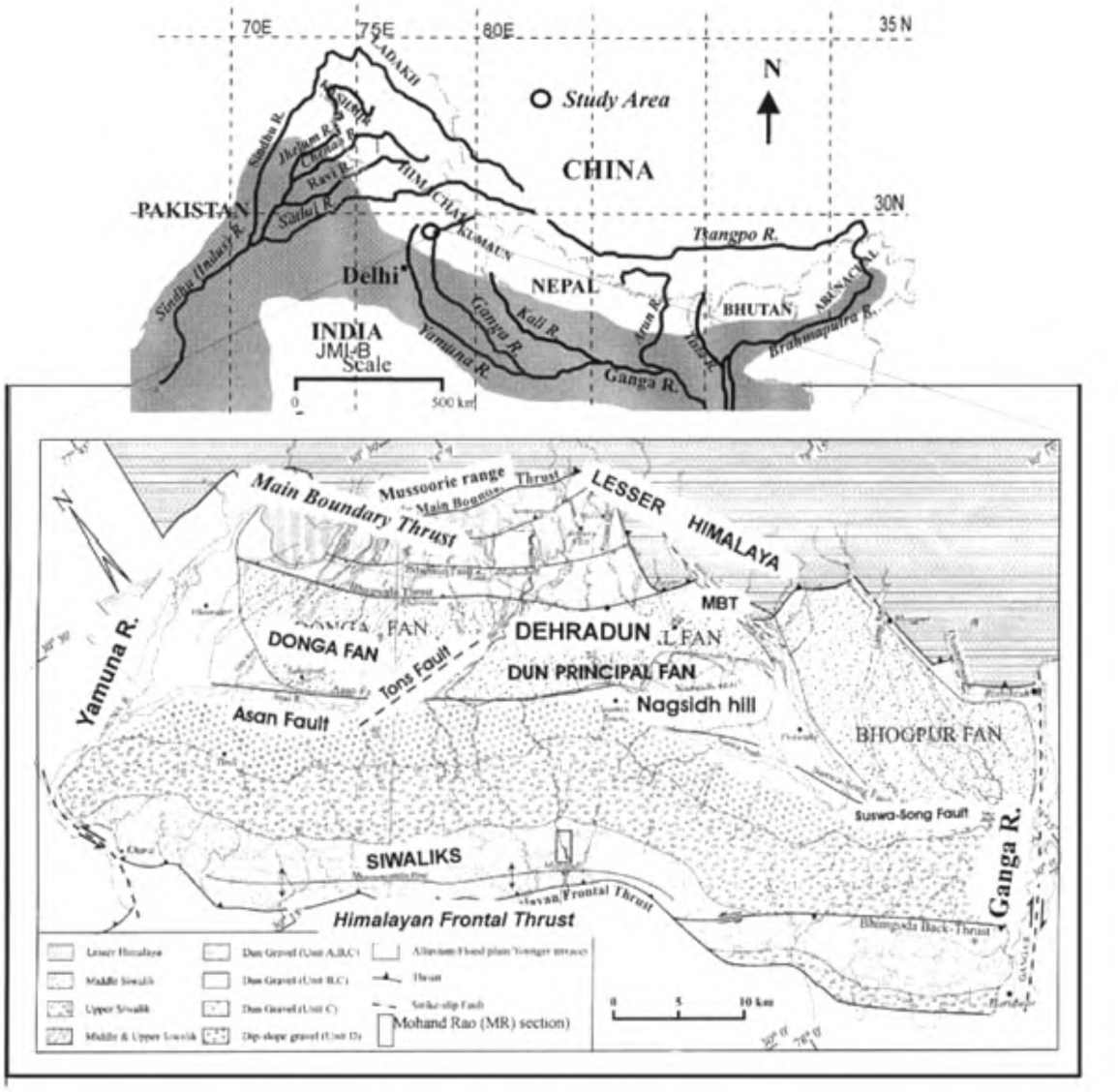

Figure 3. ***a***, Location map showing the extent of the Himalayan Foreland Basin inclusive of the Indo-Gangetic plains. ***b***, Geological map of Dehradun Sub-basin showing the Siwalik exposures (redrawn after Thakur and Pandey[27]).

strata are dipping at high angles (>20°), tilt corrections are made using equal area projections for each data to find the directions of depositional fabrics.

Petrography

Twenty representative samples were selected for the study under polarizing microscope by making two sections each parallel to and perpendicular to the field-oriented cylindrical specimen. The palaeoflow direction of the PSS is marked over the horizontal section (see white arrows in Figure 4). With detailed modal analysis, Ghosh and Kumar[13] classified these sandstones into variants of lithic arenites ($Q_{55}F_5R_{40}MX_2$), lithic graywacke ($Q_{61}F_3R_{36}MX_{24}$) and sublithic arenites ($Q_{75}F_5R_{20}MX_3$). Broadly, the sandstones vary from very fine-to-fine grained lithic graywacke from the lower part of the section to fine-to-medium grained lithic to sublithic arenites towards top.

Grain size

The mean grain size of sandstone samples ranges from 1.8 to 3.90 Phi, with a large variation in the range of very fine to medium-grained sands and contains ~4% traction, ~73% saltation and ~23% suspension loads[10,11,13]. The high percentage of suspension load in these sandstones is due to infiltration of finer clayey material into the channel sand[11]. The antiferromagnetic fraction (hematite and goethite) is abundant in the fine-grained sediments (mudstone–siltstone and palaeosols) in the MR as well as adjoining areas[26,28]. This is further evident from the present rock magnetic studies indicating the presence of antiferromagnetic mineral fractions for many of the pre-heated samples. Over-

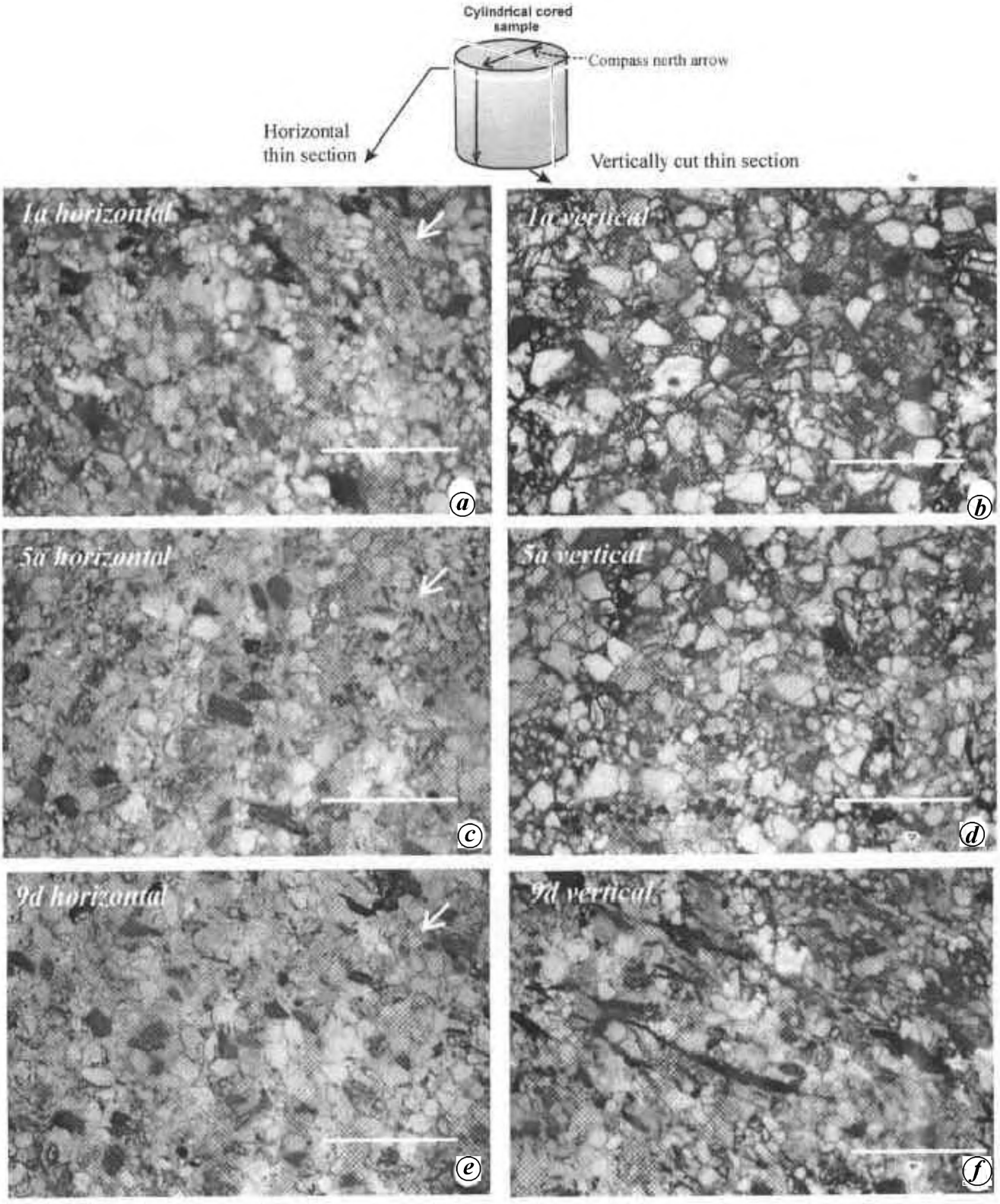

Figure 4*a–f*. Photomicrographs with representation of planes in which they were studied. (Top) Position of these planes. Arrow marks show palaeoflow direction based upon PSS. Scale = 0.288 mm in each section.

all, the grain size gradually increased up-section with individual fining upward cycles.

Mineralogy

Mineralogy is dominated by sub-angular to sub-rounded quartz (26 to 89%) of recalculated QFR modes. Sub-angular grains of plagioclase and alkali feldspars are present varying from 0 to 18%. Rock fragments of sedimentary ≫ metamorphic ≫ igneous are present in large amount (up to 50%). The rock fragments constitute < 6% basaltic and granodioritic, < 39% metamorphic (phyllitic + quartzitic + schistose), and < 55% sedimentary (shale + siltstone + sandstone + chert + limestone) fragments. Polycrystalline and elongated micaceous flakes mainly of biotite and biotite altered to chlorites are common (<16%). Heavy minerals are <5% with opaque constituents less than 2%. Particles less than 30 μm are classified as a matrix that varies from 2 to 24%. Matrix mainly consists of illite, chlorite, sericite, quartz, feldspar and mica fragments. Micaceous materials showing grain flowage are classified as pseudo-matrix[13]. Micritic to microsparitic calcite is the major cementing material followed by iron oxides and siliceous cements. Iron oxide cement consists of hematite pigment surrounding the detrital grains.

Thus the dia- and paramagnetic minerals (quartz, feldspar, micas and clay) makeup the major constituent with opaques (magnetite, hematite, ilmenite, etc.) less than 2%. Petrographic observations suggest that the preferred orientation is best shown by the micaceous minerals (biotite and chlorite, Figure 4). The opaques are mostly euhedral to anhedral and are randomly placed. Biotite and chlorite are important paramagnetic minerals that influence the AMS fabrics[17,29,30]. The mineral biotite can often contribute to ferrimagnetic susceptibilities due to ferrimagnetic (magnetite) inclusions[29,30]. The platy nature of these minerals allows them to be aligned easily due to prevailing water currents. Biotite and chlorite grains in the present samples are mostly laths and lenticels, thus producing an ideal condition to influence the fabrics.

Magnetic fabrics

The correlation matrix (Table 1) shows insignificant correlation coefficient (<0.5, with majority falling near zero and negative values) amongst the bulk mean magnetic fabric parameters (L, F, P_j, T, and the D and I values of K_1, K_2, K_3). The rose diagrams (Figure 5) also do not indicate any significant coincidence amongst the bulk mean principal susceptibility axes and the direction of the

Table 1. Correlation matrix for declination (D) and inclination (I) of the principal susceptibility axes (K_1, K_2, K_3), PSS, degree of anisotropy (P_j), lineation (L), foliation (F) and shape parameter (T), for all the PSS

	PSS–D	PSS–I	K_1–D	K_1–I	K_2–D	K_2–I	K_3–D	K_3–I	L	F	P_j	T
ALL												
PSS–D	1.0000											
PSS–I	0.1663	1.0000										
K_1–D	0.3233	–0.1119	1.0000									
K_1–I	–0.0284	–0.0430	–0.2450	1.0000								
K_2–D	–0.1775	–0.2568	–0.3017	0.0602	1.0000							
K_2–I	–0.1958	0.0857	–0.0470	–0.0689	–0.0271	1.0000						
K_3–D	–0.0290	0.2642	–0.3920	0.1873	–0.2228	–0.1135	1.0000					
K_3–I	0.2132	0.0355	0.2931	–0.7147	–0.1416	–0.5905	–0.0141	1.0000				
L	–0.2818	0.1617	–0.0233	0.0659	0.0065	–0.0346	–0.1417	–0.0159	1.0000			
F	–0.3706	–0.0638	–0.0782	–0.0523	0.1931	–0.1307	–0.2003	0.1172	0.6987	1.0000		
P_j	–0.3714	–0.0304	–0.1204	–0.0962	0.2220	–0.1129	–0.2029	0.1432	0.7093	0.9684	1.0000	
T	–0.1203	–0.4285	–0.0601	–0.0190	0.2555	–0.2335	–0.0531	0.1150	–0.4037	0.1740	0.0896	1.0000
Only TCS												
PSS–D	1.0000											
PSS–I	0.1822	1.0000										
K_1–D	0.3132	–0.0245	1.0000									
K_1–I	–0.0820	–0.1180	–0.3124	1.0000								
K_2–D	–0.1173	–0.2268	–0.3301	0.1811	1.0000							
K_2–I	–0.2284	0.1795	–0.0803	–0.0496	–0.0520	1.0000						
K_3–D	–0.0298	0.1361	–0.4016	0.2238	–0.2312	–0.0895	1.0000					
K_3–I	0.2714	0.0252	0.3591	–0.7332	–0.2136	–0.5843	–0.0514	1.0000				
L	–0.3094	0.1081	–0.0001	0.0275	0.0369	0.0187	–0.1673	–0.0330	1.0000			
F	–0.4042	–0.1661	–0.0333	0.0032	0.1334	–0.0376	–0.3596	0.0026	0.8028	1.0000		
P_j	–0.4007	–0.1221	–0.0859	–0.0639	0.1813	–0.0185	–0.3456	0.0444	0.7904	0.9597	1.0000	
T	–0.0812	–0.4303	–0.0644	0.1147	0.1523	–0.3042	–0.0765	0.0738	–0.3889	0.0761	–0.0092	1.0000

Table 2. Sites of PSS showing palaeoflow direction and eigenvalues for mean principal susceptibility axes and other fabric parameters. Cases indicate the assigned relations. Case-I, K_1 is parallel to PSS; Case-II, K_2 is parallel to PSS; Case-III, K_3 is parallel the PSS; Cases I–II, II–III, Intermediate cases where PSS lies between K_1 and K_2, K_2 and K_3 respectively. These cases are derived after plotting the K_1, K_2, K_3 and PSS directions for each sample on equal area stereonet

Site	PSS-*D*	PSS-*I*	K_1–*D*	K_1–*I*	K_2-*D*	K_2–*I*	K_3–*D*	K_3–*I*	*L*	*F*	P_j	*T*	Case
1A (TCS)	323	35	269	8	359	1	90	81	1.007	1.018	1.027	0.416	II
1C (TCS)	335	28	288	15	22	14	152	70	1.011	1.028	1.040	0.447	I
1D (TCS)	360	1	330	19	239	2	143	70	1.004	1.025	1.031	0.761	I
2A (TCS)	116	29	350	20	88	22	222	61	1.004	1.028	1.035	0.713	II
2B (TCS)	239	43	310	13	42	9	166	74	1.004	1.022	1.028	0.663	III
2C (TCS)	96	26	60	29	155	8	254	63	1.008	1.041	1.053	0.670	I
2D (TCS)	339	27	357	6	83	3	129	83	1.003	1.012	1.017	0.625	I
2E (TCS)	314	47	335	9	68	14	200	76	1.006	1.015	1.022	0.410	I
2E-1(TCS)	344	53	330	14	52	23	167	71	1.006	1.010	1.017	0.228	I
3A (TCS)	196	6	34	44	300	4	208	46	1.004	1.015	1.021	0.586	III
3B (TCS)	142	11	82	23	340	25	210	55	1.006	1.027	1.035	0.637	IV
4A (TCS)	170	55	147	35	246	11	350	53	1.027	1.083	1.118	0.504	I
5A (TCS)	220	27	321	10	228	13	64	76	1.007	1.041	1.052	0.689	II
5′A (TCS)	241	46	206	16	298	8	44	70	1.010	1.051	1.066	0.656	I
5′B (TCS)	233	39	172	14	263	8	21	72	1.011	1.046	1.061	0.616	IV
5IA (TCS)	205	20	141	15	233	7	347	72	1.009	1.031	1.042	0.541	II
5IB (TCS)	205	20	115	16	210	18	347	65	1.005	1.037	1.045	0.765	II
6A (TCS)	127	48	98	8	190	9	329	78	1.047	1.082	1.134	0.260	IV
6-OA1 (TCS)	46	1	186	6	96	6	53	81	1.028	1.145	1.191	0.661	II
6-OL1 (TCS)	208	52	136	6	229	18	29	71	1.020	1.111	1.144	0.683	II
6-OL2 (TCS)	176	33	336	27	63	10	168	61	1.040	1.093	1.053	0.523	III
6-1A (TCS)	32	9	261	15	167	12	40	71	1.038	1.117	1.167	0.500	III
6-1B (TCS)	248	6	289	8	199	5	78	81	1.028	1.103	1.141	0.564	I–II
7A (TCS)	177	54	124	13	224	37	18	50	1.019	1.051	1.074	0.447	I–II
7B (TCS)	273	17	317	6	226	11	80	77	1.023	1.081	1.111	0.574	I–II
8A (TCS)	170	33	216	20	311	15	78	65	1.016	1.071	1.093	0.642	IV
8B (TCS)	199	66	308	9	216	9	79	77	1.034	1.053	1.091	0.222	II
8C (TCS)	166	40	234	29	140	6	41	60	1.018	1.076	1.101	0.612	II
10A (TCS)	132	54	232	8	141	14	351	74	1.004	1.017	1.022	0.591	II
10B (TCS)	206	40	76	13	167	2	267	78	1.006	1.022	1.030	0.600	IV
10C (TCS)	101	22	219	14	125	20	343	64	1.008	1.014	1.023	0.257	II
12A (TCS)	116	23	271	5	179	29	10	60	1.015	1.076	1.099	0.667	IV
13A (TCS)	123	41	263	3	172	25	1	64	1.011	1.014	1.025	0.147	IV
13B (TCS)	171	38	329	1	58	2	190	88	1.006	1.024	1.032	0.593	III
13C (TCS)	181	9	283	16	186	20	46	64	1.004	1.020	1.025	0.653	II
13D (TCS)	159	33	48	3	139	21	310	69	1.007	1.021	1.029	0.521	II
13E (TCS)	170	45	176	17	83	8	331	71	1.002	1.019	1.024	0.773	I
2P (PCS)	327	43	153	6	66	4	282	86	1.006	1.020	1.027	0.580	II–III
9B (PCS)	74	5	268	5	358	0	84	84	1.004	1.052	1.063	0.847	III
11A (RDL)	212	50	241	8	148	20	351	67	1.003	1.017	1.022	0.659	I
11B (RDL)	175	53	138	10	229	4	344	80	1.015	1.162	1.201	0.820	I–III
1M (HL)	258	14	299	19	32	9	146	69	1.009	1.028	1.039	0.499	I
5C (HL)	194	4	321	22	222	19	97	60	1.006	1.029	1.038	0.684	II
5D (HL)	184	5	152	2	242	22	56	68	1.003	1.026	1.032	0.802	I–II
9C (HL)	252	3	347	5	258	15	96	74	1.008	1.078	1.096	0.796	II
9D (HL)	75	2	232	1	323	10	137	80	1.006	1.074	1.090	0.835	IV

Frequency: Case I = 11, Case II = 15, Case III = 6, Case IV = 8 and Intermediate cases = 6.

PSS except its nearness to K_2 axis. This prompted us to examine the site-specific nature of the fabric by classifying them into cases of approximation (summarized in Table 2; Figure 6). This clearly inferred a site-specific nature of the fabrics with a maximum frequency for the case II followed by cases I and IV (Table 2).

Further, we calculate subtended angles between the flow direction shown by PSS and the K_1, K_2 and K_3 directions for each site (Figure 7). It shows large mean angular difference (>60°) for K_1 and K_3 over majority of the sites with relatively lower values for the intermediate (K_2) axis. This indicates the composite nature of the fabric that may be the resultant of two or more vectors with one aligned to the palaeoflow. In the petrographic studies it was observed that the micaceous matrix minerals show better preferred orientation than the ferrimagnetic opaque minerals (Figure 4).

The matrix comprises mainly of paramagnetic minerals that contribute only to weak susceptibilities compared to ferrimagnetic minerals. In order to further investigate the possibility of any other mineral fraction aligning parallel to the palaeoflow, we apply a fabric enhancement technique described below.

Fabric enhancement study

The previous exercise has shown that majority of the magnetic fabrics are aligned intermediate to the palaeoflow (between K_1 and K_2) direction, indicating a resultant of two or more magnetic mineral phases. In a depositional environment as displayed in the MR section, the energy conditions were high and with proximal source[10]. The predominating ferrimagnetic grains (magnetite/titanomagnetites) are subhedral to anhedral with poor preferred orientations. Further, the other magnetic susceptibility influencing constituents of antiferromagnetic minerals (hematite and goethite) are poorly represented by fabrics due to their weak susceptibilities and finer grain size. However, paramagnetic minerals, especially platy varieties like mica and chlorites are more sensitive to hydrodynamic forces. Their geometries and shapes make them ideally controlled by the viscous media, thus greatly contributing to flow-related fabrics. The Mohand sandstones are rich in micaceous minerals comprising up to 15% of the modal composition with predominance of biotite. The preferred orientation of biotite grains along the flow directions (Figure 4) can thus influence the AMS fabrics, especially when the ferrimagnetic content is low and poorly oriented as in the present case.

All the magnetic minerals are temperature-sensitive and one form can be altered to the other during laboratory heating and the approach is used successfully for fabric enhancement or alteration studies[31–33]. Therefore, we heated a batch of 22 representative samples at 100, 150, 200, 300, 350, 400, 450, 500, 550, 600, 650 and 700°C for more than 25 min at each step in a thermal demagnetizer to study changes in the magnetic fabrics due to heating. AMS fabrics were measured after every step of heating till 700°C. Detailed rock magnetic studies for these samples were conducted in two steps: (a) before heating (i.e. at room temperature) and (b) after heating to 700°C. The results are described below.

Figure 8 shows the representative remanence hysteresis curves for heat treatment. Samples 1m and 5a indicate that the partial saturation isothermal remanent magnetizations (SIRMs) are unaltered even after heating up to 700°C. Interestingly, coercivity is greatly reduced after heating.

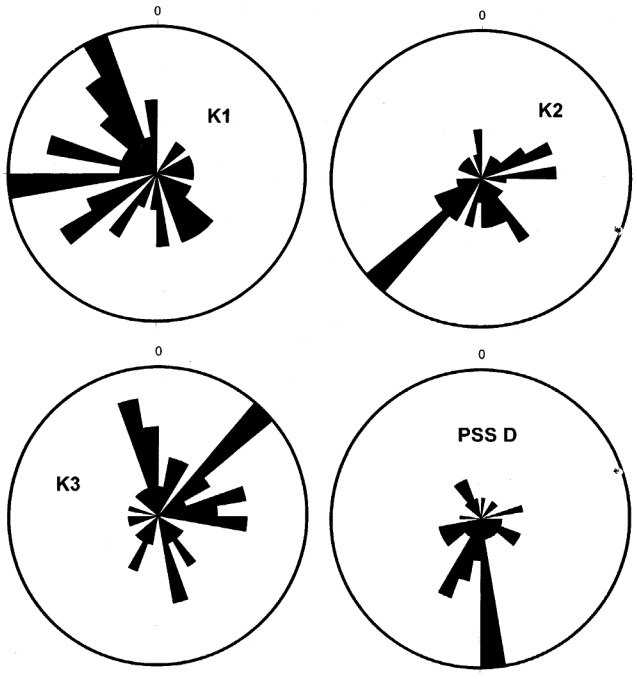

Figure 5. Rose diagram for directions of principal susceptibility ellipsoid axes and PSS. There is a large deviation of distribution for PSS from K_1, K_2 and K_3. Rose petals are represented by 10° dip direction classes.

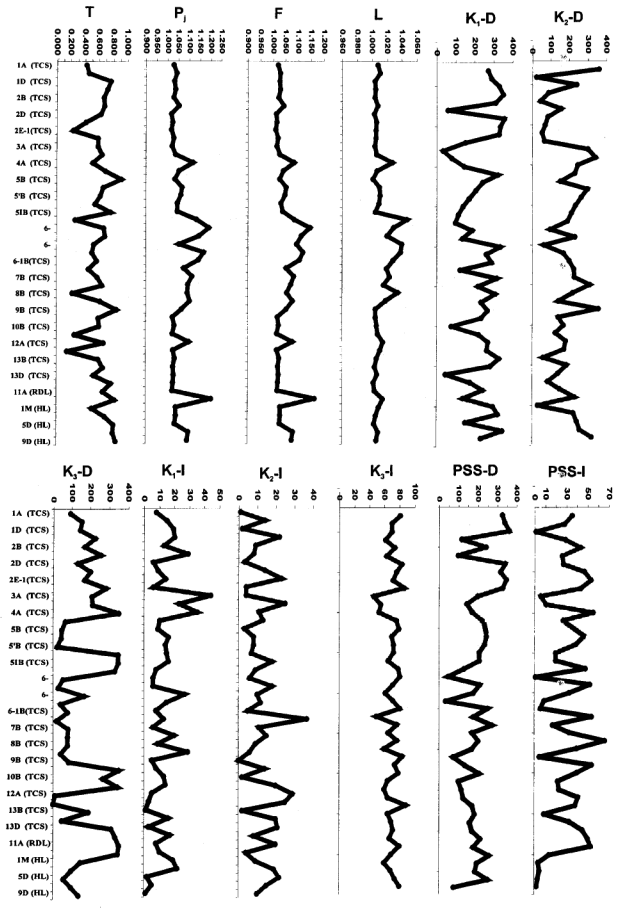

Figure 6. Magnetic fabrics and PSS parameters plotted against each site show a site-independent relation that has been classified into five cases as summarized in Table 2.

The slope of the $IRM_{forward}$ curve indicates the presence of antiferromagnetic minerals and the significant depletion of coercivity indicates multidomain (MD) or superparamagnetic (SP) fraction. It is possible to form SP fraction due to heating some of the paramagnetic minerals[32,33]. Samples 2a, 2b and 3a indicate significant increase in SIRM and decrease in coercivity due to heating. Increase in SIRM indicates addition of ferrimagnetic iron oxides, most probably due to alteration of pre-existing antiferromagnetic and paramagnetic minerals at elevated temperatures (>450°C). Samples 6OL1, 8B and 9C show significant increase in SIRMs, although the coercivity remains fairly unchanged. This indicates absence of antiferromagnetic minerals in these samples, and conversion of paramagnetic minerals into ferrimagnetic forms due to heating. In Table 3, we present the percentage degree of change after heating. The coercivities [$B_{(0)CR}$] and S-ratios for the preheated samples are remarkably reduced after heating. This indicates that the pre-existing antiferromagnetic and paramagnetic fraction is significantly altered to ferrimagnetic oxides by the heating. This is also evident from the decrease in SIRM/X_{lf} ratio and increase in X_{lf}.

The change in shape and magnitude of the fabrics with incremental heating is visualized by plotting the four major parameters (K_{lf}, volume susceptibility; P_j, degree of anisotropy; T, shape of the ellipsoid and K_1–D, direction of the principle susceptibility axis in Figure 9). For the sample 1A-8, K_{lf}, P_j and T increase after 450°C, attain a peak at 550°C and then drop afterwards. The K_1–D values show large fluctuations till 450°C, and then follow a trajectory beyond 550°C, indicating a direction that coincides with the palaeoflow. This indicates a significant addition of new iron oxides by 450°C, most probably due to oxidation of the pre-existing mineral matrix along the bedding laminea of the troughs (TCS). Similar trends are also shown by samples 1C-8, 1m-4 and 2A-7. K_{lf} for 2B-4 too shows similar peak as above, however P_j and T values do not follow any peak at 550°C. In this sample, K_1–D is also not entirely affected by heat treatment. The S-ratio for this sample indicates an addition of antiferromagnetic oxide due to heating, without altering the anisotropy. Sample 2P-8 shows a peak at 550°C for K_{lf} and P_j but T and K_1–D are fairly constants similar to sample 2B-4. Sample 3A-10 shows gradual rise in K_{lf} after 450°C, simultaneous with P_j and K_1–D becoming steady beyond 450°C. This indicates strong anisotropy due to formation of ferrimagnetic oxides after 450°C. However, it does not correspond with the palaeoflow directions even after heating. Samples 5A-3 and 5′A-3 show large fluctuations in K_{lf} and a peak in P_j at 650°C, although T and K_1–D remain fairly unaltered (K_1–D fluctuates at the boundary of the first and fourth quadrants). This indicates the complex behaviour of iron oxide transformation at various temperature levels affecting the AMS for these samples. K_{lf} for samples 5C-5 and 5IA-2 shows a minor peak, in contrast to a very high peak for P_j at 650°C. T does not show any major peak, but gradually increases during incremental heating. K_1–D for this sample shows a steady trend towards 360° after heating to 600°C and mimics the direction of the palaeoflow. Sample 6OL1-1D shows minor humps in K_{lf}, P_j and T after 600°C, but K_1–D steadily moves towards the first quadrant deviating from the palaeoflow direction. Sample 6OL1-2C shows gradually declined K_{lf}, large fluctuations in P_j and steady trend for K_1–D towards the fourth quadrant without matching the palaeoflow direction. Sample 6-1A-3 indicates steady rise in K_{lf}, P_j and T after 500°C and the K_1–D becomes 360° at 700°C. Samples 7A-3 and 8B-6 show gradual decrease in K_{lf}, but P_j rises suddenly after 500°C. Sample 9C-5 shows increase in K_{lf}, P_j and T after 500°C. Samples 13E-2 and 13C-1 show large change in K_{lf} and P_j after 450°C. T remains steady, while K_1–D becomes stable near the boundary of the first and fourth quadrants after heating to 200°. P_j shows a major peak matching with susceptibility at 550°C for sample 13B-1, without any significant change in K_{lf} and K_1–D does not match with the palaeoflow.

Heat treatment has shown that the fabrics are altered significantly only after 450°C. These changes show simultaneous increase in the K_{lf}, P_j and T around 550°C. In general, they indicate increase in oblateness and eccentricity of the fabric. The degree of foliation (F) is also greatly enhanced for these samples (not plotted in Figure 9).

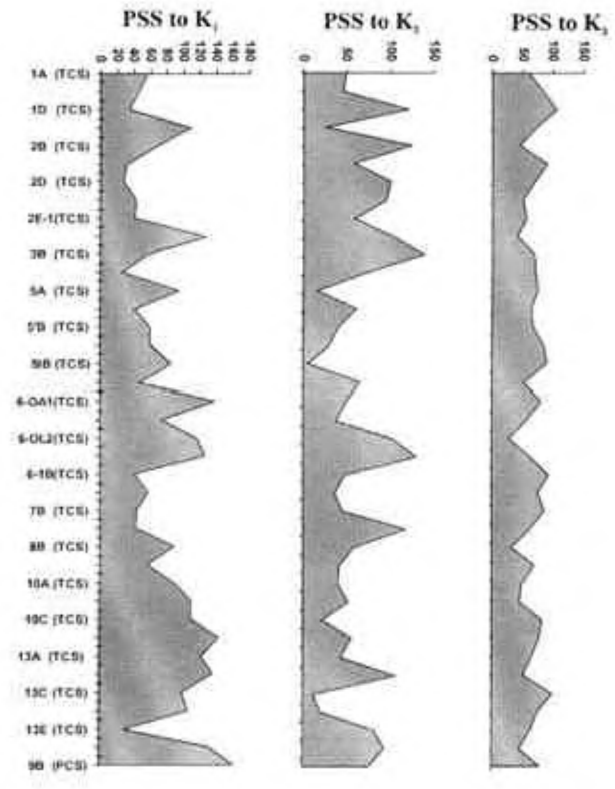

Figure 7. Subtended angles (in degrees) between PSS and the principal susceptibility axes (K_1, K_2 and K_3) at representative site locations (plotted as vertical axis).

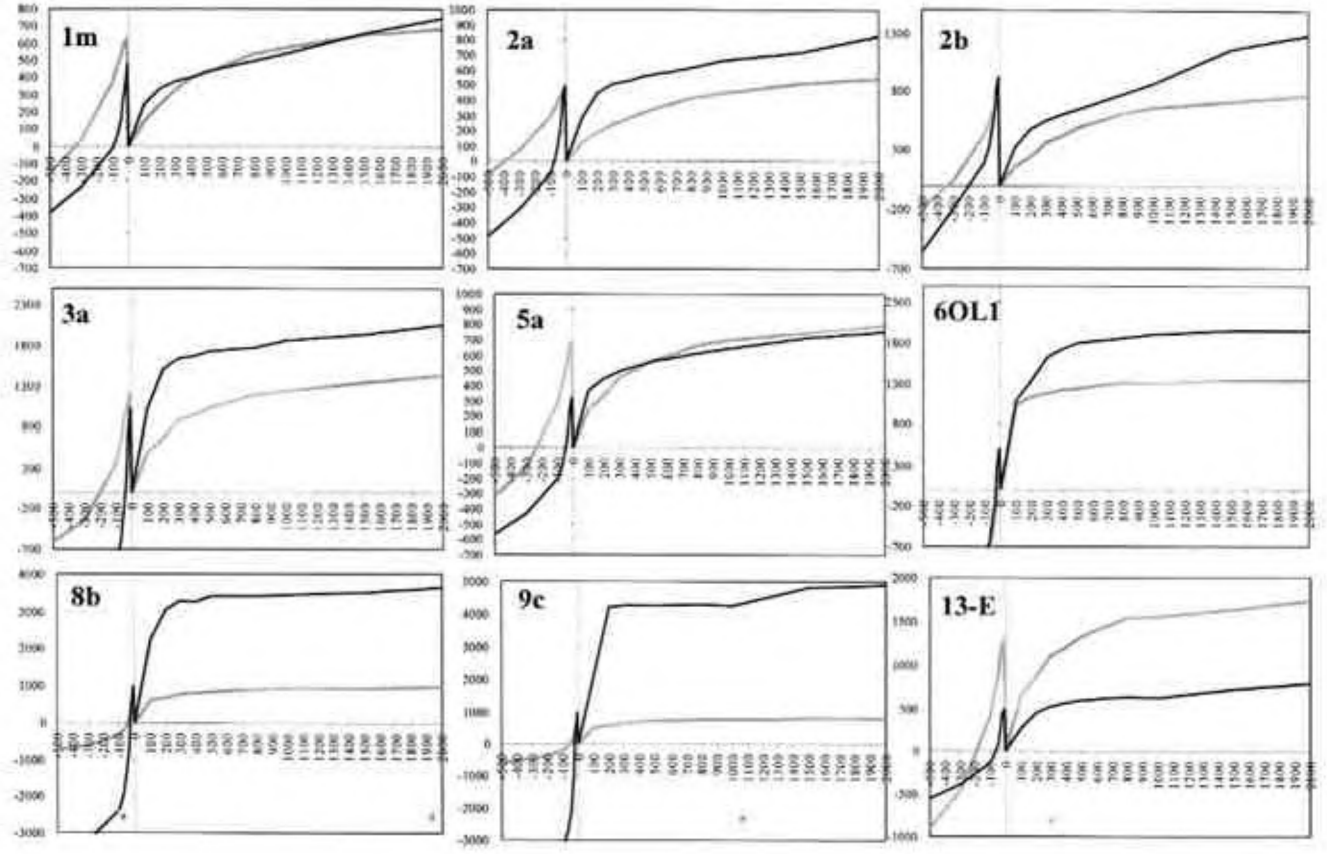

Figure 8. Remanence hysteresis loop for pre-heated (grey) and heated to 700°C (black) treatment of IRM. Note significant change in back field coercivity parameter that suggests transformation of canted antiferromagnetic minerals into ferrimagnetic (see text for details).

Table 3. Selective rock magnetic parameters showing pre-heated values followed by succeeding columns (asterisk mark) for heated values (700°C). Percentage change due to heating treatment is also shown

Sl. no.	BoCR	BoCR*	Δ%	XLF	Xlf*	%	SIRM/Xlf	SIRM/X*	Δ%	S-Ratio	S-Ratio*
13b1	240	64	–73	0.27	0.50	85	114.69	91.99	–19	0.33	–0.18
13-E1	195	69	–64	0.51	0.38	–24	147.35	97.72	–33	0.23	–0.16
13C-1	195	52	–73	0.47	0.34	–26	106.41	198.50	86	0.20	–0.29
1A-8	215	270	25	0.47	2.19	363	250.68	27.86	–88	0.35	0.25
1C-8	275	215	–21	0.35	3.81	986	142.12	10.11	–92	0.48	0.19
1M-4	340	100	–70	0.31	1.67	442	91.54	18.53	–79	0.55	–0.01
2A-7	385	78	–79	0.26	2.76	955	83.89	12.41	–85	0.55	–0.09
2B-4	330	195	–40	0.37	0.59	61	86.80	87.51	1	0.56	0.15
2P-8	310	197	–36	0.41	0.35	–14	137.34	159.69	16	0.57	0.15
3A-10	200	42	–79	0.48	0.53	10	119.87	164.02	36	0.25	–0.45
5′A-3	26	33	26	8.31	0.34	–95	5.02	715.39	14153	–0.56	–0.48
5C-5	210	158	–24	0.36	0.40	10	173.34	73.67	–57	0.28	0.10
5IA-2	158	55	–65	0.44	0.46	4	142.60	113.62	–20	0.15	–0.25
60L1-2C	20	32	60	2.49	0.59	–76	23.12	137.02	492	–0.61	–0.44
60L1-D1	32	47	46	1.89	1.92	1	33.45	244.98	632	–0.35	–0.37
61A-3	25	34	36	1.35	3.44	155	19.32	32.37	67	–0.45	–1.37
7A-3	18	25	38	4.12	0.58	–85	31.42	650.98	1972	–0.71	–0.66
8B-6	45	26	–42	0.98	0.88	–9	40.62	172.68	325	–0.35	–0.65
9C-5	60	22	–63	0.59	0.51	–14	56.16	419.06	646	–0.26	–0.65

As discussed earlier, rock magnetic studies have indicated the formation of ferrimagnetic oxides (e.g. magnetite) and/or SP fractions from pre-existing paramagnetic and/or antiferromagnetic minerals due to heating. Increase in K_{lf} beyond ~450°C to reach a peak at ~550°C for majority of the samples, suggests the formation of ferrimagnetic oxides

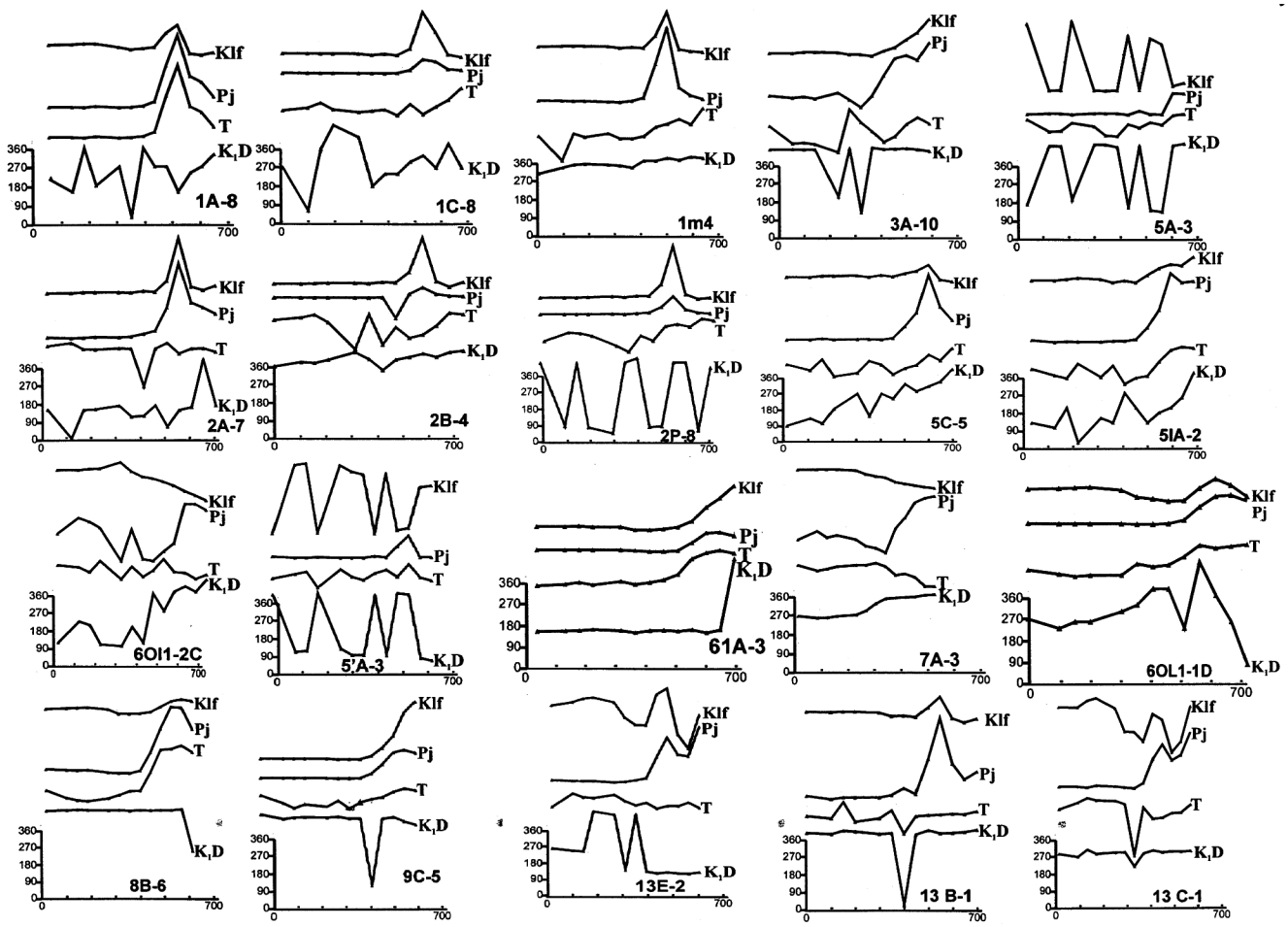

Figure 9. Change in magnetic fabrics with stepwise heating shown by various parameters.

from paramagnetic constituent minerals. Increase in the foliations and their coincidence with K_1–D suggest that fabric enhancement mainly occurred along the bedform laminae of the primary structures.

Conclusion

Magnetic fabric studies from the high-energy Nagri channel sequence of Dehradun Sub-basin in the HFB are indicative of composite nature of fabrics resulting from poorly oriented ferrimagnetic and fairly well-oriented paramagnetic mineral constituents. Petrographic studies have inferred that the paramagnetic constituents greatly outnumber the ferrimagnetic minerals, showing preferred orientation to the flow direction. The AMS is therefore a resultant of paramagnetic and ferrimagnetic mineral alignments at room temperature and laboratory heating above 450°C can further enhance the fabrics along the bedform laminae by oxidation of majority of paramagnetic and antiferromagnetic minerals.

This study indicates that the principle susceptibility ellipsoid axis (K_1) becomes sub-parallel to the palaeoflow under high-energy, proximal to medial-braided river environments in the HFB due to the composite nature of magnetic fabrics. These fabrics can be referred to as 'depositional fabrics' resulting out of (i) preferred orientation of paramagnetic mineral matrix, and (ii) shape fabric due to ferrimagnetic mineral grains. The depositional fabrics can be controlled by energy conditions (stream power), clast composition and grain geometry that are in turn governed by tectonic and climatic changes in the proximal foreland setting like in the present study area. Changes in these conditions are reflected by the change in fabric parameter that can be inferred for relative quantification of magnitudes of tectonic and/or climatic impulses. Since the AMS instrumental technique is highly sensitive and rapid, it provides a better quantitative and qualitative approach to model the fluvial responses to tectonic and climatic changes. More detailed studies are required to relate the grain size, grain geometries and energy conditions to the shape and intensity of magnetic fabrics by studying the varied fluvial depositional

environment in the older as well as modern records available in the HFB and the Indo-Gangetic foredeep.

1. Allen, J. R. L., *Current Ripples. Their Relation to Patterns of Water and Sediments Motion*, North Holland, Amsterdam, 1968, p. 433.
2. Allen, J. R. L., *Sedimentary Structures*, Elsevier, 1982, vol. 30A, p. 593.
3. Singh, I. B., Geological evolution of Ganga Plain – An overview. *Palaeontol. Soc. India J.*, 1996, **41**, 99–137.
4. Gibling, M. R., Tandon, S. K., Sinha, R. and Jain, M., Discontinuity-bounded alluvial sequence of the southern Gangetic plains, India: Aggradation and degradation in response to monsoonal strength. *J. Sediment. Res.*, 2005, **75**, 373–389.
5. Reineck, H. E. and Singh, I. B., *Depositional Sedimentary Environments*, Springer-Verlag, Berlin, 1973.
6. Collinson, J. D. and Thompson, D. B., *Sedimentary Structures*, George Allen & Unwin, UK, 1982, p. 194.
7. Willis, B., Ancient river system in the Himalayan foredeep, Chinji village area, northern Pakistan. *Sediment. Geol.*, 1993, **88**, 1–76.
8. Willis, B., Evolution of Miocene fluvial systems in the Himalayan foredeep through a two kilometer-thick succession in northern Pakistan. *Sediment. Geol.*, 1993, **88**, 77–121.
9. Kumar, R., Ghosh, S. K. and Sangode, S. J., Role of thrusting in the evolution of fluvial system, Himalayan Foreland Basin, India. In *Himalaya and Tibet: Mountain Roots to Mountain Tops* (eds MacFarlane, A., Sorkhabi, R. B. and Quade, J.), Geol. Soc. Am., Spec. Pap., 1999, vol. 328, pp. 239–256.
10. Kumar, R., Sangode, S. J. and Ghosh, S. K., A multistorey sandstone complex in the Himalayan Foreland Basin, NW Himalaya, India. *J. Asian Earth Sci.*, 2004, **23**, 407–426.
11. Kumar, R. and Nanda, A. C., Sedimentology of the Middle Siwalik Subgroup of Mohand area, Dehra Dun valley, India. *J. Geol. Soc. India*, 1989, **34**, 597–616.
12. Kumar, R. and Ghosh, S. K., Evolution of Mio-Pleistocene alluvial fan system in the Siwalik Foreland Basin, Dehra Dun, India. *Himalayan Geol.*, 1994, **15**, 143–159.
13. Ghosh, S. K. and Kumar, R., Petrography of Neogene Siwalik sandstones of the Himalayan foreland basin, Garhwal Himalaya: Implications for source area tectonics and climate. *J. Geol. Soc. India*, 2000, **55**, 1–15.
14. Tarling, D. H. and Hrouda, F., *The Magnetic Anisotropy of Rocks*, Chapman and Hall, London, 1993, 1st edn, p. 217.
15. Hernandez-Martin, F., Luneburg, C. Aubourg, C. and Jackson, M. (eds), *Magnetic Fabric: Methods and Applications*, Geological Society London Special Publications, 2004, p. 560.
16. Jelinek, V., Characterization of magnetic fabrics of rocks. *Tectonophysics*, 1981, **79**, 637.
17. Borraidale, G. J. and Henry, B., Tectonic applications of magnetic susceptibility and its anisotropy. *Earth Sci. Rev.*, 1997, **42**, 49–93.
18. Borradaile, G. J., Magnetic susceptibility, petrofabrics and strain. *Tectonophysics*, 1988, **156**, 1–20.
19. Ellwood, B. B., Particle flocculation – one possible control on the magnetization of deep sea sediments. *Geophys. Res. Lett.*, 1979, **6**, 237–240.
20. Sangode, S. J., Kumar, R. and Ghosh, S. K., Application of magnetic fabric studies in an ancient fluvial sequence of NW Himalaya. *Curr. Sci.*, 2001, **81**, 66–71.
21. Piper, J. D. A., Elliot, M. T. and Kneller, B. C., Anisotropy of magnetic susceptibility in a Palaeozoic flysch basin: The Windermere Supergroup, northern England. *Sediment. Geol.*, 1996, **106**, 235–258.
22. Bouchez, J. L., Hutton, D. H. W. and Stephens, W. E., *Granite: From Segregation of Melt to Emplacement Fabrics*, Kluwer, 1997, p. 356.
23. Sangode, S. J., Kumar, R. and Ghosh, S. K., Palaeomagnetic and rock magnetic perspectives on the post-collision continental sediments of the Himalaya. In *Indian Subcontinent and Gondwana: A Palaeomagnetic and Rock Magnetic Perspective* (eds Radhakrishna, T. and Piper J. D. A.), Memoir Geological Society of India, 1999, vol. 44, pp. 221–248.
24. Allen, J. R. L., Asymmetrical ripple marks and the origin of water-lain cosets of cross-strata, *Liverpool Manchester Geol. J.*, 1963, **3**, 187–234.
25. Sangode, S. J., Magnetostratigraphy and sedimentation history of the Siwalik foreland basin in Dehra Dun Nahan sector, NW Himalaya. D Phil thesis, HNB Garhwal University, 1997, p. 152.
26. Kumaravel, V., Sangode, S. J., Siva Siddaiah, N. and Rohtash Kumar, Rock magnetic characterization of pedogenesis under high energy depositional conditions: A case study from the Mio–Pliocene Siwalik fluvial sequence near Dehra Dun, NW Himalaya, India. *Sediment. Geol.*, 2005, **177**, 229–252.
27. Thakur, V. C. and Pandey, A. K., Active deformation of Himalayan Frontal Thrust and piedmont zone south of Dehradun in respect of seismotectonics of Garhwal Himalaya. *Himalayan Geol.*, 2004, **25**, 25–31.
28. Sangode, S. J. and Bloemendal, J., Pedogenic transformation of magnetic minerals in Pliocene–Pleistocene palaeosols of the Siwalik Group, NW Himalaya, India. *Palaeogeogr. Palaeoclimatol. Palaeoecol.*, 2004, **212**, 95–118.
29. Rochette, P., Metamorphic control of the magnetic mineralogy of black shales in the Swiss Alps: toward the use of 'magnetic isograde's'. *Earth Planet. Sci. Lett.*, 1987, **84**, 446–456.
30. Rochette, P., Magnetic susceptibility of the rock matrix related to magnetic fabric studies. *J. Struct. Geol.*, 1987, **9**, 1015–1020.
31. Perarnau, A. and Tarling, D. H., Thermal enhancement of magnetic fabric in Cretaceous sandstone. *J. Geol. Soc. London*, 1985, **142**, 1029–1034.
32. Souque, C., Robion, P. and Frizon de Lamotte, D., Cryptic magnetic fabric of tectonic origin revealed by heating sedimentary samples from the Corbieres. *Phys. Chem. Earth*, 2002, **27**, 1253–1262.
33. Henry, B., Jordanova, D., Jordanove, N., Souque, C. and Robion, P., Anisotropy of magnetic susceptibility of heated rocks. *Tectonophysics*, 2003, **366**, 241–258.

ACKNOWLEDGEMENTS. We are grateful to Prof. B. R. Arora, Director, Wadia Institute of Himalayan Geology, Dehradun for suggestions, discussion and encouragement. We thank Dr V. C. Tewari for providing facilities and suggestions. This work was carried out under the research grant funded by Department of Science and Technology, New Delhi.

Received 31 January 2006; revised accepted 23 October 2006